AGU PUBLICATIONS

JGR

Journal of Geophysical Research: Atmospheres

RESEARCH ARTICLE

10.1002/2016JD025285

Key Points:

- Surface T in every region will reach a new climate norm well before mid 21st century regardless of the magnitudes of regional warming
- Clausius-Clapeyron scaling exists at regional scales where per degree C rise in surface T will lead to a 7.4% increase in P from extremes
- Both winter (snow) and summer (liquid) extremes are projected to increase across the U.S.

Supporting Information:

- Supporting Information S1

Correspondence to:
M. Ashfaq,
mashfaq@ornl.gov

Citation:
Ashfaq, M., D. Rastogi, R. Mei, S.-C. Kao, S. Gangrade, B. S. Naz, and D. Touma (2016), High-resolution ensemble projections of near-term regional climate over the continental United States, *J. Geophys. Res. Atmos.*, *121*, doi:10.1002/2016JD025285.

Received 27 APR 2016
Accepted 11 AUG 2016
Accepted article online 13 AUG 2016

High-resolution ensemble projections of near-term regional climate over the continental United States

Moetasim Ashfaq[1,2], Deeksha Rastogi[1,2], Rui Mei[1,2], Shih-Chieh Kao[2,3], Sudershan Gangrade[2,3], Bibi S. Naz[2,3], and Danielle Touma[4]

[1]Computer Science and Mathematics Division, Oak Ridge National Laboratory, Oak Ridge, Tennessee, USA, [2]Climate Change Science Institute, Oak Ridge National Laboratory, Oak Ridge, Tennessee, USA, [3]Environmental Sciences Division, Oak Ridge National Laboratory, Oak Ridge, Tennessee, USA, [4]Department of Earth System Science, Stanford University, Stanford, California, USA

Abstract We present high-resolution near-term ensemble projections of hydroclimatic changes over the contiguous U.S. using a regional climate model (RegCM4) that dynamically downscales 11 global climate models from the fifth phase of Coupled Model Intercomparison Project at 18 km horizontal grid spacing. All model integrations span 41 years in the historical period (1965–2005) and 41 years in the near-term future period (2010–2050) under Representative Concentration Pathway 8.5 and cover a domain that includes the contiguous U.S. and parts of Canada and Mexico. Should emissions continue to rise, surface temperatures in every region within the U.S. will reach a new climate norm well before mid 21st century regardless of the magnitudes of regional warming. Significant warming will likely intensify the regional hydrological cycle through the acceleration of the historical trends in cold, warm, and wet extremes. The future temperature response will be partly regulated by changes in snow hydrology over the regions that historically receive a major portion of cold season precipitation in the form of snow. Our results indicate the existence of the Clausius-Clapeyron scaling at regional scales where per degree centigrade rise in surface temperature will lead to a 7.4% increase in precipitation from extremes. More importantly, both winter (snow) and summer (liquid) extremes are projected to increase across the U.S. These changes in precipitation characteristics will be driven by a shift toward shorter and wetter seasons. Overall, projected changes in the regional hydroclimate can have substantial impacts on the natural and human systems across the U.S.

1. Introduction

While global climate modeling is scientifically the most sophisticated approach to study the climate response due to changes in various forcing factors, there exist large uncertainties in the global climate model (GCM)-based future climate projections at regional scales. Despite the significant advancements in climate modeling since the first Intergovernmental Panel on Climate Change (IPCC) Assessment in 1990 [*Houghton et al.*, 1990], the typical resolution of a GCM in the Fifth Assessment Report (AR5) is still coarser than 150 km, which is insufficient to simulate the response of the subtle, local-scale climate processes and feedbacks that govern climate change at fine spatial and temporal scales [e.g., *Ashfaq et al.*, 2009; *Diffenbaugh et al.*, 2005; *Meir et al.*, 2006; *Suggitt et al.*, 2011]. The lack of advancement toward higher-resolution GCMs is partly hampered by the fact that centennial-scale high-resolution GCM experiments are demanding both scientifically and computationally and need substantial improvements in the representation of the fine-scale processes and feedbacks, as well as in the numerical algorithms for parallel computational architectures. Therefore, as the magnitude and distribution of hydroclimatic extremes are sensitive to the horizontal grid spacing of the climate models [e.g., *Hagos et al.*, 2015; *Lu et al.*, 2014; *Wehner et al.*, 2010], the current generation of GCMs is not very skillful in the projection of regional climate change and hydroclimatic extremes, particularly over regions of complex topography. Hence, the direct use of GCM-based projections is not appropriate for reliable regional to local scale climate impact assessments and policymaking.

Currently, the scale mismatch issues can be addressed by embedding a regional climate model (RCM) within a GCM at a relatively finer resolution over the region of interest [*Giorgi and Mearns*, 1999]. The GCM outputs are treated as initial and boundary conditions during the RCM simulation. Because RCMs are configured over a limited area, it is relatively less cumbersome to tune these models than global-scale GCMs. Moreover, the higher spatial resolution of RCMs provides better representation of physical processes and fine-scale feedbacks, especially over topographically complex and spatially heterogeneous regions. Of course, regional climate modeling has its own limitations and is in no way a substitute for GCMs in the simulation of the Earth system's response to variations in climate forcing. One of the major drawbacks in the regional modeling approach is the artificial lateral boundaries and the lack of feedback between the RCM (regionally refined domain) and the driving GCM (rest of the globe), which may influence the simulated model responses within the finer domain. Moreover, the RCM's skill heavily depends on the quality of the boundary forcing (provided by the driving GCM) in the representation of large-scale climate processes. Likewise, it should also be noted that RCM simulations are very time consuming and scientifically challenging and require experienced modelers to ensure that the GCM signals can be faithfully downscaled. Given these limitations, the number of RCM ensemble members and the size of the regional model domain are generally constrained.

In this study, future climate projections over the continental U.S. are based on the dynamical refinement of the resolution of GCMs climate projections that are the basis of the Fifth Assessment Report (AR5) of *Intergovernmental Panel on Climate Change* [2013]. An ensemble of high-resolution regional climate change experiments is generated by dynamically downscaling GCMs using a one-way nesting approach. With this approach, a high-resolution regional climate model is forced at its lateral and lower boundaries every 6 h using three-dimensional atmospheric and two-dimensional surface fields from low-resolution GCMs, while no feedback is permitted from the regional climate model to the driving GCMs. Many modeling efforts in the past have used dynamical downscaling for regional climate projections over the U.S. For instance, *Diffenbaugh et al*. [2005] employed a single RCM to downscale a single GCM over the continental U.S. at 25 km horizontal grid spacing. Similarly, using the identical domain, horizontal grid spacing, and model configuration, *Diffenbaugh and Ashfaq* [2010] used a single RCM to downscale multiple integrations of a single GCM and generated a centennial-scale five-member ensemble of climate projections over the continental U.S. Additionally, in a multiinstitutional effort, the North American Regional Climate Change Program (NARCCAP) used a combination of six RCMs and four GCMs over a domain covering North America at 50 km horizontal grid spacing and generated a 12-member multi-RCM ensemble of climate projections [*Mearns et al*., 2009]. Likewise, many other studies used high-resolution subregional RCM domains to provide high-resolution short time-slice projections of the hydroclimate over various parts of the continental U.S. [e.g., *Duffy et al*., 2006; *Fan et al*., 2014; *Gula and Peltier*, 2012; *Salathe et al*., 2010]. However, in terms of the number of downscaled GCMs, horizontal grid spacing, and the length of simulations, the regional climate modeling in this study is perhaps one of the largest dynamical downscaling efforts over the continental U.S. to date. Overall, these experiments have utilized over 10 million computational hours on the Titan supercomputer maintained by the Oak Ridge Leadership Computing Facility at Oak Ridge National Laboratory and have generated over 100 terabytes of subdaily three-dimensional hydrometeorological projections.

This study mainly focuses on the details of the dynamical downscaling, the modeling skill of the RCM in the historic period and future projections of the mean annual and extreme daily precipitation and surface temperature at the subregional scale over the continental U.S. and should serve as a reference for future research efforts using this data.

2. Methods

2.1. Regional Climate Modeling

We employ Abdus Salam International Centre for Theoretical Physics Regional Climate Model version 4 (RegCM4) to dynamically downscale multiple GCMs from the fifth phase of Coupled Model Intercomparison Project (CMIP5) archive over the continental U.S. Details of the RegCM4 nested climate model are described in *Giorgi et al*. [2012]. RegCM4 is a hydrostatic, sigma coordinate, primitive equation, and limited-area model. In our configuration, RegCM4 uses the hydrostatic dynamical core from Fifth Generation Mesoscale Model (MM5) [*Grell et al*., 1994], the radiation package from Community Climate Model version 3 (CCM3) [*Kiehl et al*., 1998], the Community Land Model (CLM) version 3.5 [*Tawfik and Steiner*, 2011], and the Holtslag boundary layer package [*Holtslag et al*., 1990]. Precipitation processes are parameterized using the Subgrid Explicit Moisture Scheme (SUBEX) scheme of *Pal et al*. [2000] and the cumulus convection parameterization of *Grell* [1993] with the closure assumption of *Fritsch and Chappell* [1980]. The earlier version of this model (RegCM3), which mainly differs from the current version in the parameterizations of land surface processes [*Pal et al*., 2007], has been successfully used a number of times for dynamically downscaling GCMs over the U.S. [e.g., *Ashfaq et al*., 2010, 2013; *Diffenbaugh and Ashfaq*, 2010; *Diffenbaugh et al*., 2005, 2011; *Mearns et al*., 2009].

Table 1. Summary of the 11 Dynamically Downscaled CMIP5 GCMs

No.	GCM Name	Spatial Resolution (latitude/longitude)	Ensemble Number	Institute Name
1	ACCESS1-0	1.24°/1.88°	r1i1p1	Commonwealth Scientific and Industrial Research Organization (CSIRO) and Bureau of Meteorology (BOM), Australia
2	BCC-CSM1-1	2.81°/2.81°	r1i1p1	Beijing Climate Center, China Meteorological Administration
3	CCSM4	0.94°/1.25°	r6i1p1	National Center for Atmospheric Research
4	CMCC-CM	0.75°/0.75°	r1i1p1	Centro Euro-Mediterraneo per I Cambiamenti Climatici
5	FGOALS-g2	3.00°/2.81°	r1i1p1	LASG, Institute of Atmospheric Physics, Chinese Academy of Sciences and CESS, Tsinghua University
6	GFDL-ESM2M	2.00°/2.50°	r1i1p1	Geophysical Fluid Dynamics Laboratory
7	MIROC5	1.41°/1.41°	r1i1p1	Atmosphere and Ocean Research Institute (The University of Tokyo), National Institute for Environmental Studies, and Japan Agency for Marine-Earth Science and Technology
8	MPI-ESM-MR	1.88°/1.88°	r1i1p1	Max Planck Institute for Meteorology (MPI-M)
9	MRI-CGCM3	1.13°/1.13°	r1i1p1	Meteorological Research Institute
10	NorESM1-M	1.88°/2.50°	r1i1p1	Norwegian Climate Centre
11	IPSL-CM5A-LR	1.88°/3.75°	r1i1p1	Institut Pierre-Simon Laplace

In this study, the RegCM4 grid is centered at 39.00°N and 100.00°W and consists of 202 points in the latitude direction and 306 points in the longitude direction. Grid points are separated by 18 km horizontally and have 18 levels in the vertical. The Lambert Conformal projection places the grid corners at 50.17°N, 138.86°W (northwest), 50.10°N, 60.91°W (northeast), 19.58°N, 125.44°W (southwest), and 19.53°N, 74.40°W (southeast). In total, 11 GCMs from Coupled Models Intercomparison Project Phase 5 (CMIP5) archives are downscaled to generate 11 sets of historical and future realizations under the Representative Concentration Pathway 8.5 (RCP 8.5). RCP 8.5 exhibits the highest levels of forcing and global warming at the end of the 21st century, with a radiative forcing reaching ~8.5 W m^{-2} and greenhouse gas concentrations exceeding 1370 ppm CO_2 equivalent [*Moss et al*., 2010]. In each set of RegCM4 simulations, the historical baseline period consists of 41 years from 1965 to 2005 and the projected future period consists of 41 years from 2010 to 2050. The first year of RegCM4 simulation in both the baseline and future periods is used for model spin up and has been discarded in the analysis.

Each RegCM4 ensemble member uses the same parameterization options, with only large-scale input varying between the RegCM4 ensemble members. Details about the modeling institute, GCM resolution and future forcing are provided in Table 1. The choice of CMIP5 GCMs is mainly based on the availability of subdaily three-dimensional atmospheric data needed for dynamical downscaling. While there are over 50 GCMs that contributed to CMIP5, less than one third of them archive three-dimensional atmospheric fields at the sub-daily time scale, which is necessary for dynamical downscaling. Also, though a few GCMs had more than one ensemble member data available for downscaling, we only used one ensemble simulation per GCM for consistency. We focus on RCP 8.5 since it is closest to the current observed trajectory. Given that the difference among various RCPs becomes significant only after 2030 [*Peters et al*., 2013], the choice of RCP is potentially not a dominating factor in the near-term climate projection.

2.2. Observational Data

For baseline comparisons, observational monthly and daily temperature and precipitation data sets are taken from the Parameter-Elevation Regressions on Independent Slopes Model (PRISM) at 4 km horizontal resolution [*Daly et al*., 2008] and Oak Ridge National Laboratory Daymet at 1 km horizontal grid resolution [*Thornton et al*., 2014]. While PRISM data are available at a monthly time scale for the entire length of the baseline period, daily PRISM and Daymet data sets are only available after 1980. Therefore, the estimation of all the simulation errors is only for the time period (1981–2005) for which both daily and monthly gridded observational data are available.

2.3. Analysis

We perform analysis at the annual time scale for the characterization of the mean climate and at the daily time scale for the characterization of climate extremes. Results are also presented both at the continental scale and the regional scale. All continental-scale results are presented as the mean of ensemble members. For regional-scale comparisons, we divide the continental U.S. into nine climate regions using the classification defined by the National Centers for Environmental Information (NCEI) [*Karl and Koss*, 1984]. Commonly used terminologies (e.g., northeast, Great Lakes, and Great Plains) are used to describe the results over different regions. NCEI climate region names are only used while describing the regionally averaged results.

All future projections are reported as change from 1981–2005 baseline to 2011–2050 future periods. Transient climate projections are based on the differences of individual years both in the baseline and future periods from the reference period (1981–2005). We present these analyses for both observations (Daymet and PRISM) and simulations (entire length of baseline and future simulations). We also perform trend analysis on the annual anomalies using the rank based Mann-Kendall test [*Kendall*, 1975; *Mann*, 1945] to quantify the significance of temporal changes in the baseline (for both observations and simulations) and future periods (simulations). Trends are calculated for the overlapping periods (1981–2005) in the baseline and for the entire length of the projections period in the future.

For the calculation of precipitation extremes, we first define a wet day when the daily amount of precipitation is at least 1 mm/d. We then use the climatological value of the 95th percentile of wet day precipitation, calculated as an average of the 95th percentile during each year of the comparison period, as a threshold for precipitation extremes. Using identical methodology, snow extremes are calculated for each year for the snow days that occur during 1 October to 31 March. Similarly, for temperature extremes, we use the climatological value of 95th (5th) percentile of maximum (minimum) daily temperature, calculated as an average of the 95th (5th) percentile during each year of the comparison period, as a threshold for hot (cold) extremes. While the use of 1 mm/d threshold for the selection of wet days is not uncommon, we note that it may substantially reduce number of wet days over relatively drier regions in the western U.S. and impact the results for future changes in precipitation extremes over those regions.

In order to quantify changes in precipitation seasonality, we use the methodology described in *Feng et al*. [2013]. For each hydrological year (October to September), we calculate the seasonality of precipitation as a multiplicative product of relative entropy, which quantifies the extent of precipitation concentration in the wet season, and annual mean precipitation normalized by the domain maximum over the length of the analyses period. Further changes in the timing and duration are calculated using the first and second moments of annual mean rainfall, respectively. Timing or the first moment is the centroid of the rainfall distribution when 50% of the annual precipitation is reached in a hydrological year. Duration or the second moment is the temporal deviation from the centroid of the rainfall and is useful to quantify the changes in the length of the wet season. In this study, we calculate these quantities for each hydrological year in the baseline and future periods and average the results over the respective lengths of simulations. In order for the results to be comparable across different grid points (continental U.S.), data sets (observations, model simulations), and simulation periods (baseline, future), we normalize the results using the maximum rainfall value found over all data sets and simulation periods. Further details of the methodology and mathematical expressions can be referred to *Feng et al*. [2013].

We use several measures to determine the robustness or uncertainty of the simulated results across the ensemble members. First, all spatial maps are stippled over the grid points where seven or more GCMs agree on the threshold (only in the case of temperature) or the sign of the projected changes. Second, we perform trend analysis to test the significance and consistency of temporal changes in the individual ensemble members and the ensemble mean. Third, we use box and whisker plots to describe the spread among the ensemble members in their simulated future changes.

3. Results and Discussion

3.1. Representativeness of the Selected GCMs

In order to investigate the representativeness of the selected CMIP5 GCMs (11 in total; hereafter GCM-SUB) that have been downscaled in this study, we compare their ensemble mean annual precipitation and temperature projections (for RCP 8.5) with a larger set of CMIP5 GCM projections (37 in total; hereafter GCM-ALL). Here the selection of 37 GCMs in GCM-ALL is mainly based on the availability of both temperature and precipitation data at the time of analysis. The percentage change in annual precipitation, percent of GCMs with positive precipitation change, and the projected change in annual temperature are shown in Figure 1.

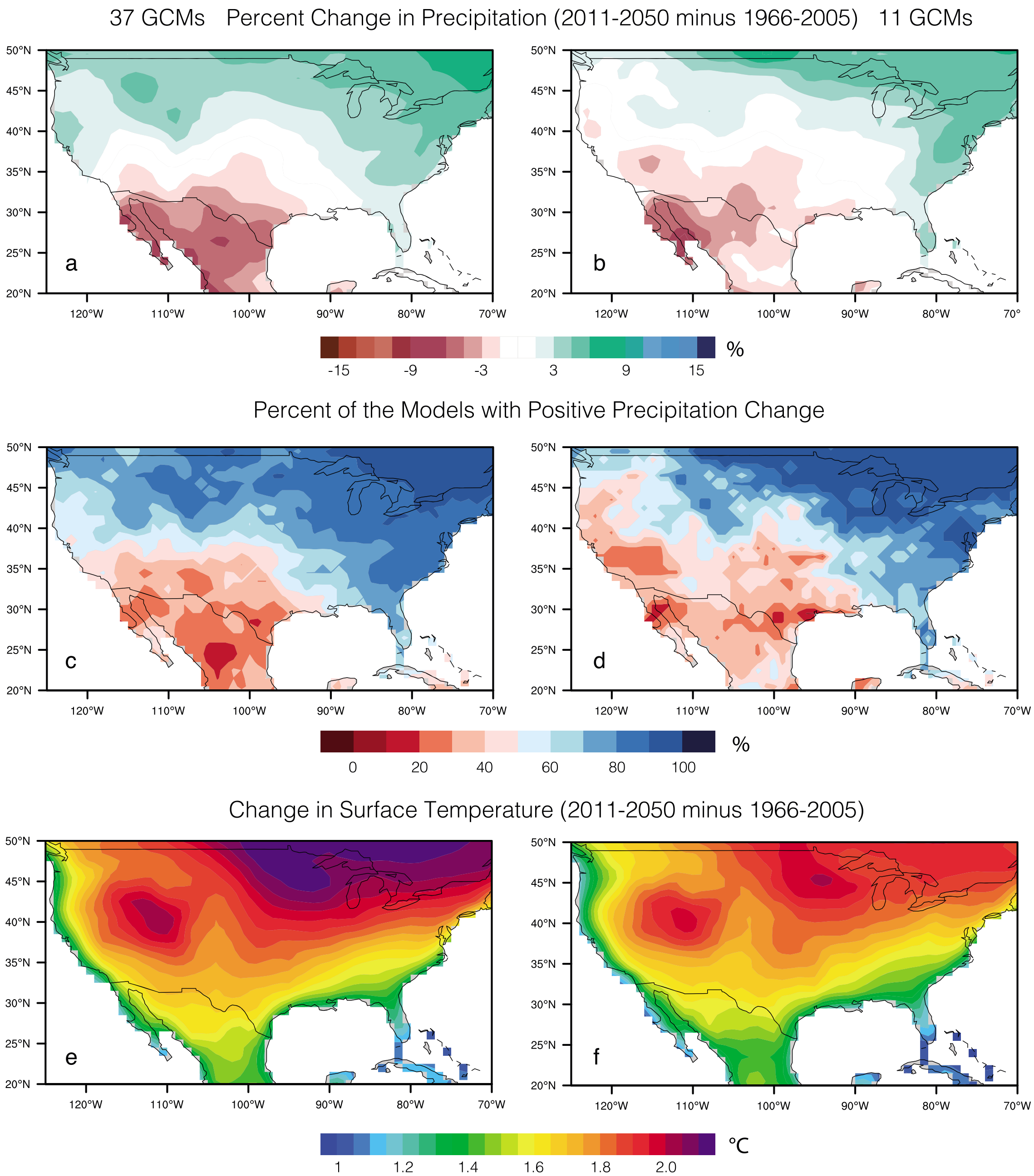

Figure 1. Comparison of multimodel ensemble projections made by (a, c, and e) 37 CMIP5 GCMs (GCM-ALL) and the selected (b, d, and f) 11 CMIP5 GCMs (GCM-SUB). The percentage change in annual precipitation is shown in Figures 1a and 1b. The percent of GCMs with positive precipitation change is summarized in Figures 1c and 1d. The projected change in annual temperature (°C) is shown in Figures 1e and 1f. Changes are based on the difference of 40 years average in the future period (2011–2050) from 40 years average in the baseline period (1966–2005).

With the exception of the southwest region, GCM-ALL simulates a robust increase in precipitation in the future period that gradually intensifies in magnitude from the south to the north (Figure 1a). GCM-SUB simulates a similar precipitation change with the exception of the northwest region where the response is generally muted in contrast to the increase in GCM-ALL (Figure 1b). The differences over the northwest are mainly due to the fact that only 30 to 60% of the GCMs in GCM-SUB simulate an increase in precipitation over the northwest compared to 50 to 80% of GCMs in GCM-ALL (Figures 1c and 1d). Temperature increases in both the ensembles exhibit a similar spatial pattern with generally mild increases along the coasts in the south and west (up to 1.5°C) and stronger increases over the snow dominant regions in the west and north (up to 2°C). However, GCM-ALL exhibits relatively stronger increases of greater than 2°C in the north over parts of Canada

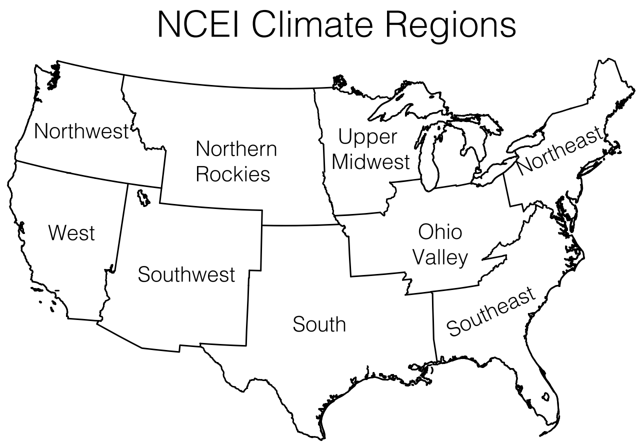

Figure 2. National Centers for Environmental Information (NCEI) climate regions.

and northern Great Plains (Figures 1e and 1f). Slightly lower magnitudes of warming (up to ~0.3°) in GCM-SUB can be partly attributed to the relatively stronger magnitudes of precipitation increases over those regions compared to GCM-ALL (Figure 1). Nonetheless, GCM-SUB simulates a response generally consistent with GCM-ALL and does not represent the outliers in the CMIP5 data.

3.2. Added Value by RCMs

To comprehensively evaluate modeling skills of the downscaled RegCM4 ensemble (hereafter RCM-SUB) against the observations and driving GCMs (GCM-SUB), we use Taylor diagrams [*Taylor*, 2001] that summarize the performance of eight variables, including mean precipitation, mean temperature (daily maximum, minimum, and average), precipitation extremes (average annual 95% percentile), temperature extremes (average annual 95% and 5% percentiles), and the number of wet days, for each of the nine NCEI climate regions (Figure 2). Comparisons are based on the normalized statistics from 1981 to 2005 where both daily PRISM and Daymet data sets are available. We evaluate the modeling skills in separate Taylor diagrams, one each for GCM-SUB and RCM-SUB with PRISM and one each for GCM-SUB and RCM-SUB with Daymet. Comparisons are made first at a 1° resolution (Figure 3) for the large-scale patterns and at the RegCM4 grid resolution (18 km) for the fine-scale details (Figure 4). The Taylor diagram quantitatively compares the pattern correlation, the ratio of variance (ROV), and the root-mean-square difference (RMSD) between the simulation (GCM or RCM) and the observation (Daymet or PRISM). The radial coordinates represent the ROV and RMSD: ROV as the radial distance from the reference arc (labeled with a dotted arc) and RMSD as the radial distance from the point of reference (labeled Daymet or PRISM). Similarly, the angular coordinate represents the pattern correlation, which measures the extent to which maxima and minima in the reference data (i.e., observations) and the test data (i.e., simulations) occur at a similar location.

Both at large and fine scales, GCM-SUB exhibits large errors in the ROV and RMSD for temperature and precipitation extremes over most of the regions (Figures 3 and 4). Similarly, pattern correlation for hot daily surface temperature extremes and number of wet days is below 0.6 over most regions and is in between 0.5 and 0.9 on the average across all variables (Figures 3 and 4). In both large- and fine-scale comparisons, the high-resolution downscaled RCM-SUB exhibits an improvement in the characteristics of both mean annual and extreme daily temperature and precipitation over all regions. For instance, the pattern correlation is in between 0.6 and 0.95 on average across all variables in RCM-SUB (Figures 3 and 4). Similarly, errors in ROV and RMSD for extreme daily surface temperature and extreme daily precipitation are relatively lower than those in GCM-SUB. Overall, we find an improvement in RCM-SUB over GCM-SUB in at least two out of three (ROV, RMSD, and pattern correlation) characteristics for 90% of the comparisons. These results highlight the added value of the high-resolution RCM-SUB, particularly in the simulation of both large-scale patterns and fine-scale details of extreme temperature and precipitation thresholds. Such improvements in RCM simulations over the driving GCMs are well known and have been reported in previous RCM studies over North America [e.g., *Leung and Qian*, 2003; *Liang et al.*, 2008; *Mearns et al.*, 2012; *Plummer et al.*, 2006; *Walker and Diffenbaugh*, 2009].

3.3. Regional Climate Projections

Figure 5 shows the projected changes in the mean annual temperature and precipitation, hot, cold and wet extremes, and number of wet days. The overall spatial patterns of simulated changes in the mean annual temperature in RCM-SUB are generally consistent with the original projections from GCM-SUB (Figures S1 in the supporting information and 5). RCM-SUB simulates pronounced warming (up to 1.7°C) over the higher elevations in the western U.S. and parts of the northern U.S. and milder temperature increases over the

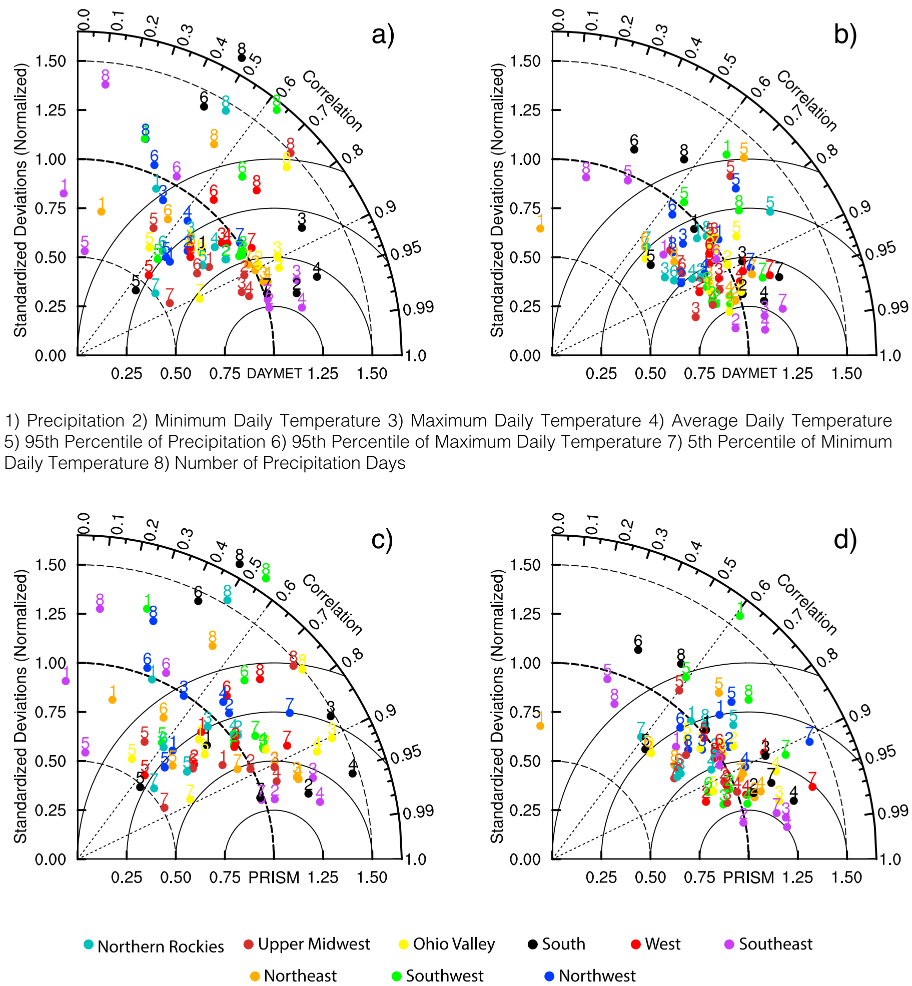

Figure 3. Comparison of (b, d) the RegCM4 ensemble (RCM) and (a, c) the driving GCMs ensemble (GCM-SUB) with Daymet (Figures 3a and 3b) and PRISM (Figures 3c and 3d) observations through Taylor diagrams. Comparison is based on the statistics derived from 1981 to 2005 period when gridded daily temperature and precipitation are available. Both the observations and the simulations (GCM-SUB, RCM) are regridded at 1° resolution for evaluation.

southeastern U.S. (up to 1.1°C, Figure 5a). The warming magnitudes over the southeast region are relatively weaker in RCM-SUB compared to GCM-SUB (Figures S1 and S2). While we did not analytically quantify the physical mechanisms for these differences between the driving GCM-SUB and the downscaled RCM-SUB, it should be noted that GCM-SUB exhibits the largest errors in the distribution of annual precipitation over this region (Figures 3 and 4), which may partly contribute to the stronger future surface temperature response. Nonetheless, the temperature increase in RCM-SUB is associated with strong increases in extreme hot days over the western U.S., along the east coast and parts of southeastern U.S., as well as decreases in extreme cold days over the south-southwestern and northeastern U.S. (Figures 5b and 5c). Most of the strong changes in extreme hot and cold days in RCM-SUB are simulated by at least 60% of the models (represented by the stippled regions, Figures 5b and 5c). Moreover, in many of the regions where both extreme hot and cold days exhibit strong changes in at least 60% of the ensemble members, the warming is expected to exceed 2°C with respect to the 1981–2005 average in the last decade (2040s) of projected future period, shown as the stippled regions in Figure 5a. However, it should be noted that the magnitude of decrease in the number of cold extremes is almost 3 times lower than that of the increase in the number of hot extremes, indicating that changes in the hot extremes are a major driver of the increases in mean temperatures, which is consistent with earlier findings [e.g., *Meehl et al.*, 2009; *Melillo et al.*, 2014].

In comparison to GCM-SUB, precipitation changes are stronger and understandably more spatially variable in RCM-SUB, particularly over west-northwestern regions where the more accurately resolved higher elevations

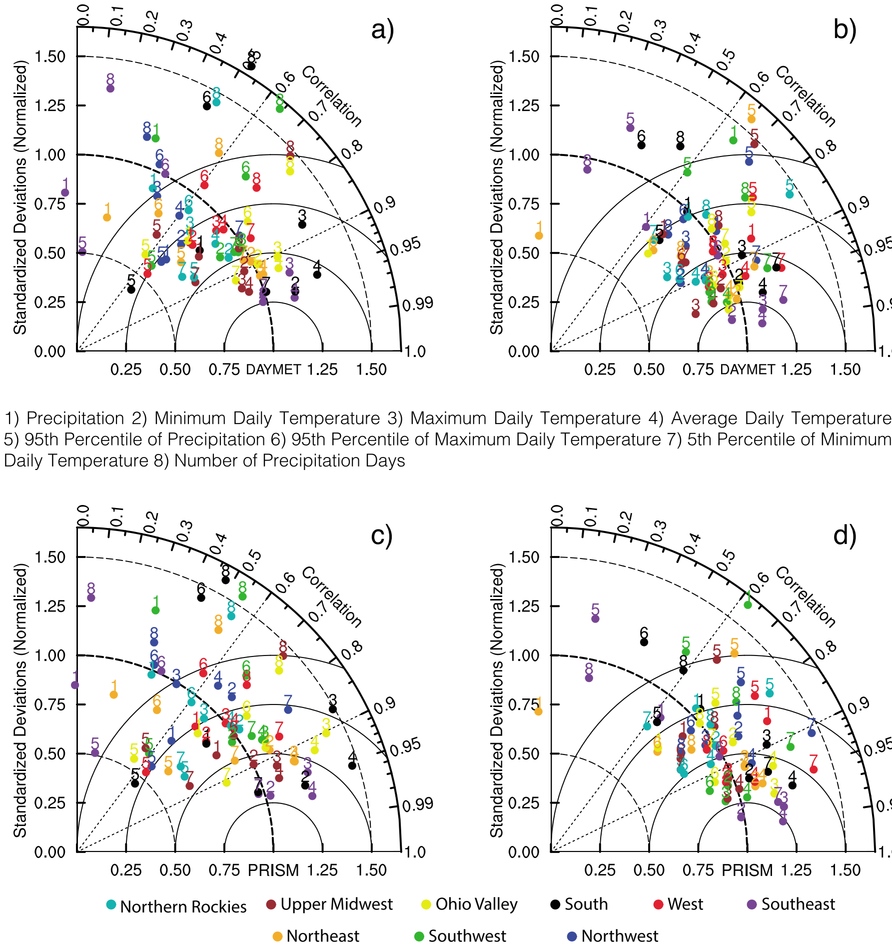

Figure 4. Same as Taylor diagram comparison in Figure 3 but with observations, GCM and RCM simulated regridded at the RegCM4 resolution (~18 km) for evaluation.

in the RegCM4 ensemble are projected to experience increase in precipitation (up to 10%, Figures S1 and 5d). Other notable differences in the precipitation response occur over parts of the northeast and south where RCM-SUB simulates a decrease of up to 6%, which is opposite in sign to the precipitation changes in GCM-SUB (Figures S1 and 5d). Here we should point out that RCM-SUB is least skillful over the northeast in the distribution of annual precipitation (Figures 3 and 4), which may partly influence simulated future precipitation response and differences with the driving GCM-SUB (Figure 5d). Regardless of the mean annual precipitation response in RCM-SUB, precipitation is expected to occur less frequently but more intensely almost everywhere (Figures 5e and 5f). Interestingly, even regions with the strongest decrease in the mean annual precipitation mostly exhibit an increase in the precipitation extremes (e.g., southwest; Figure 5). Similarly, regions with the largest increase in precipitation extremes (>10% per decade) coincide with regions that have the largest increases in mean annual precipitation (e.g., higher elevations, Great Lakes; Figure 5). As is the case with temperature changes, regions where over 60% of the models agree in mean annual precipitation changes (stippled areas) also exhibit stronger changes in precipitation characteristics, namely, magnitude (Figure 5d), occurrence (Figure 5e), and intensity (Figure 5f).

Changes in future precipitation are further examined by variations in the seasonal distribution and interseasonal variability of precipitation. Using the seasonality analyses developed by *Feng et al*. [2013], we illustrate the seasonality, entropy, timing of 50% annual precipitation and duration of the wet season for both observations and simulations in Figure 6, and their projected changes in Figure 7. We note that seasonality can be large if entropy and/or annual magnitudes of precipitation are large as seen over the west coast, northwest, south, and parts of Great Plains (Figure 6a). Higher values of entropy suggest little to no rain outside of the

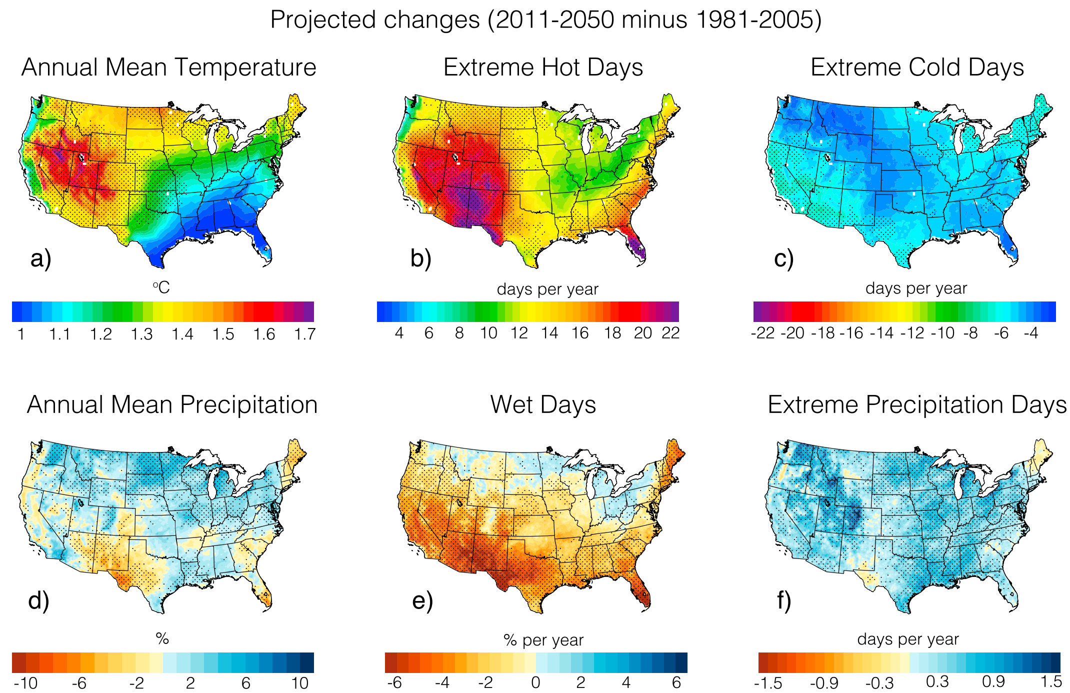

Figure 5. Projected change by the RegCM4 ensemble, from 1981–2005 baseline to 2011–2050 future periods: (a) annual mean temperature (°C), (b) number of extreme hot days (days per year), (c) number of extreme cold days (days per year), (d) change of annual precipitation (%), (e) number of wet days (% per year), and (f) number of extreme precipitation days (days per year). Stippling in Figures 5d–5f represents grid points where seven or more models agree on the sign of the change. Stippling in Figure 5a represents grid points where seven or more models simulate at least 2°C warming in the last future decade (2041–2050). Stippling in Figure 5b (Figure 5c) represents grid points where seven or more models simulate at least 10 (5) more (less) extreme hot (cold) days per year in 2011–2050.

wet season as in California, southwest, and Great Plains (Figure 6b). Regions where annual precipitation magnitudes are relatively moderate but where precipitation is well distributed across the year (high number of precipitation days) [*Walker and Diffenbaugh*, 2009] exhibit low seasonality values such as parts of the northeast and Great Lakes region. Other hatched regions exhibit low seasonality solely due to the lack of precipitation (Figure 6a) and the results for seasonality analysis should be ignored over those regions. Timing reflects the wettest time during the hydrological year, starting in October in this analysis. For instance, most of the precipitation in the western U.S. (Great Plains) is during the winter (spring and summer) season(s), which is reflected in the relatively early (late) timing for 50% annual precipitation. Alternatively, the midyear timing (~180 days) for the southeast highlights the fact that precipitation is relatively uniformly distributed during the entire year (Figure 6c). Similarly, the duration of the wet season is comparatively short over California and parts of Great Plains (Figure 6d), which can partly explain their higher vulnerability to droughts. Most of the above mentioned subannual characteristics of precipitation are reasonably simulated by RCM-SUB except for a few exceptions such as the east coast (southwest) where precipitation is relatively less (more) distributed across the months (Figure 6). Another exception exists along the parts of Gulf Coast where wet precipitation biases drive stronger than observed seasonality in RCM-SUB. Overall, these biases in the seasonality and entropy lead to errors in the timing for 50% annual precipitation and overall length of the wet season. Future projections in precipitation characteristics suggest important changes in the distribution of precipitation at monthly to seasonal time scales. With the exception of the northern Great Plains, Upper Midwest, and Florida, there is a general shrinking of wet seasons across the U.S. (Figure 7c), regardless of the sign of change in the magnitudes of annual precipitation (Figure 7d). This shrinking of wet seasons is manifested by an increase in the seasonality and the entropy (Figures 7a and 7b) and a decrease in the number of precipitation days (Figures 5e). In parts of California and the northwest, shorter rainy seasons are expected to shift the timing of 50% annual precipitation occurrence date up to 5 days earlier. On the other hand, in the southern Great Plains and parts of the southeast, a precipitation shift toward the later half of the hydrological year (not shown) delays the timing of 50% annual precipitation occurrence date by up to

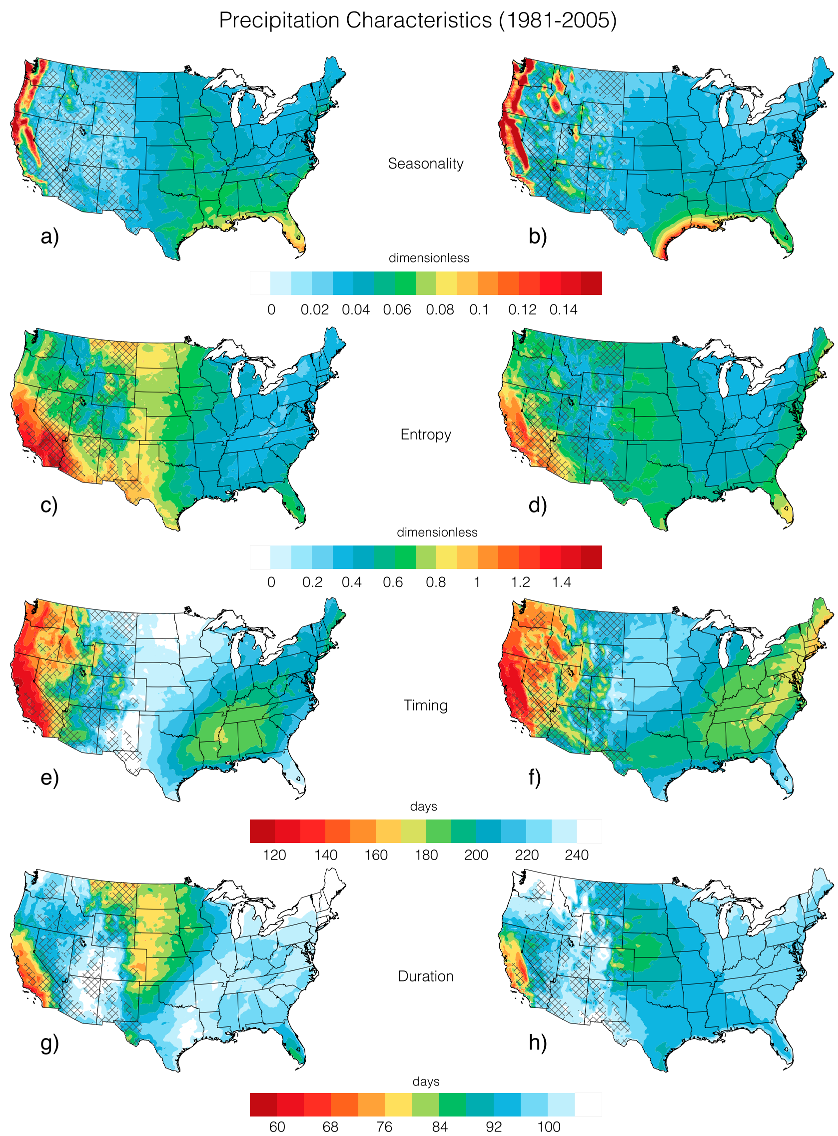

Figure 6. (a, c, e, and g) Precipitation characteristics in observations and (b, d, f, and h) RegCM ensemble. Seasonality (Figures 6a and 6b), relative entropy (Figures 6c and 6d), timing (Figures 6e and 6f), and duration (Figures 6g and 6h). Observations are based on the average of PRISM and Daymet. Hatching represents the regions where annual mean precipitation is <1 mm/day.

5 days (Figure 7d). Delays in the timing over parts of the northeast and Florida are driven more by a decrease in the annual precipitation (Figures 5d and 7d).

3.4. Uncertainty Across Ensemble Members

In order to understand regional-scale uncertainty in the projected hydroclimate changes across RCM-SUB members, we use box and whisker plots for each of the nine NCEI climate regions (Figure 8). For each region and each member of RCM-SUB, we calculate the mean and extreme values at each grid point integrated over the two time periods and the results are presented as spatial averages of the projected changes using all the grid points within that region. We calculate the projected change as the difference between the 40 year mean of the future period (2011–2050) and the 25 year mean of the baseline (1981–2005) period.

In the case of temperature, the southeast exhibits the smallest increases and spread among the ensemble members with a median increase of <1.2°C and range of <0.4°C (Figure 8a). Relatively small increases are also

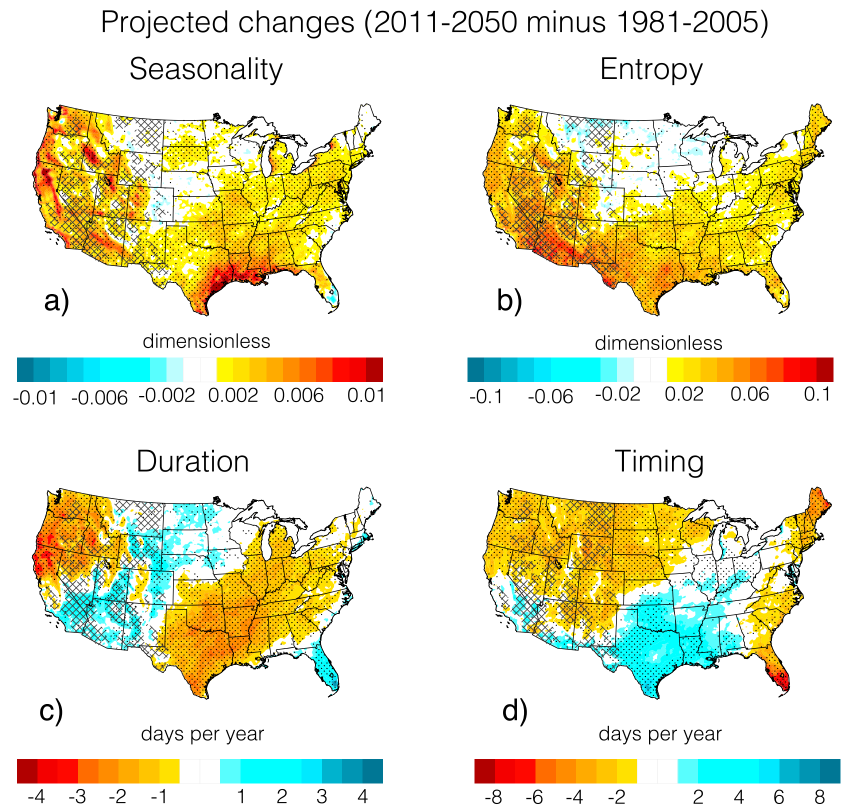

Figure 7. Future changes (2011–2050 minus 1981–2005) in RegCM4 ensemble for (a) magnitude of seasonality, (b) relative entropy, (c) duration of wet season, and (d) timing of 50% annual precipitation. Hatching represents the regions where annual mean precipitation is <1 mm/day.

projected over the south and Ohio Valley with a median warming of <1.4°C. On the other hand, the southwest and west exhibit the strongest increase in temperature with more than half of the ensemble members showing warming of >1.6°C. Regions in the northern U.S. (Northwest, northern Rockies, and Upper Midwest) exhibit the largest spread among the models (Figure 8a), which partly explains why many of these regions do not show high model agreement in reaching the 2°C warming in 2040s despite having a relatively higher magnitude of mean warming (Figure 5a, nonstippled regions). Regions with the strongest median warming (southwest and west; >1.7°C) are also the regions where the median increase in extreme hot days is the highest (>18 days), though the southwest also exhibits one of the largest spreads among the models. Interestingly, the southeast exhibits the least mean warming (Figure 8a) but the third highest median increase in extreme hot days (Figure 8b), which is in part due to its low summer temperature variance [*Diffenbaugh and Ashfaq*, 2010]. On the other hand, the Ohio Valley and the Upper Midwest exhibit the minimum increases in extreme hot days, which is consistent with the observed trends [*Portmann et al*., 2009]. The projected decreases in the number of extreme cold days are approximately less than half of the projected increases in the number of extreme hot days, which is consistent with the observed changes in the hot and cold extremes [*Meehl et al*., 2009]. Some of the largest median changes in cold extremes occur over the southwest and west (−7 days or more), consistent with strong increases in mean temperatures and number of extreme hot days, and some of the mildest median changes occur over the northern Rockies (−5 days), consistent with relatively strong increases in precipitation (Figure 5d). Additionally, the interensemble spread for extreme cold days is relatively lower than that for extreme hot days (Figure 8).

As for precipitation, the strongest ensemble median (>3%) and robust increase in precipitation occur in the Upper Midwest and northern Rockies where almost all the ensemble members simulate an increase in precipitation (Figure 8d). On the other hand, the west and southwest are the only two regions where more than half of the ensemble members exhibit a decrease in precipitation while the southeast exhibits the smallest projected changes in precipitation with the largest number (3) of outliers. The largest spread among the

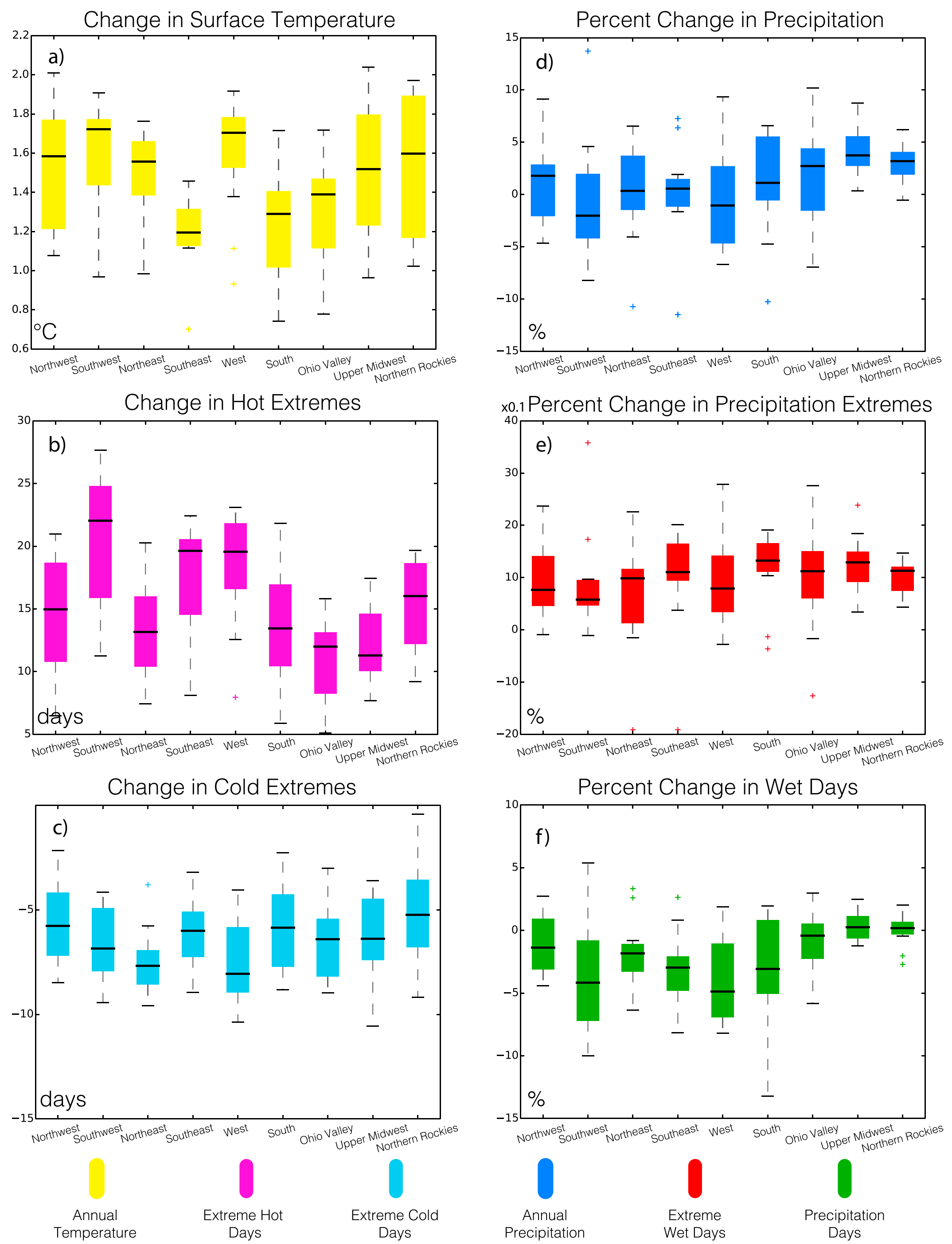

Figure 8. Box and whisker plots showing the spread of projected changes across RegCM4 ensemble members in each NCEI region for (a) average annual temperatures (°C), (b) number of extreme hot days (days per year), (c) number of extreme cold days (days per year), (d) annual precipitation (%), (e) precipitation extremes (%), and (f) number of wet days (%). Changes are based on the differences of 2011–2050 future period from 1981 to 2005 baseline period. The range of the RCM-SUB is shown, where the center line in the box is the 50th percentile of the ensemble, the bottom and top boundaries of the box represent the 25th and 75th percentiles, respectively, and the crosses show the outliers which fall approximately outside the 99th percentile of the RCM ensemble.

ensemble members occurs in the west, Ohio Valley, and northwest with differences between the minimum and the maximum projected precipitation changes exceeding 12% (Figure 8d). While the mean precipitation response is heterogeneous across the U.S., the projected changes in the number of precipitation extremes is robust, as almost all the models show an increase in days where the daily precipitation magnitude exceeds the climatological value of the 95th percentile of the baseline precipitation (Figure 8e). The characteristics of the projected change in the number of precipitation extremes across the regions are quite consistent with those of the percent change in mean annual precipitation. For instance, the northwest, west, and Ohio Valley show a larger range of projected changes in both the mean annual precipitation and precipitation extremes across the ensemble members (Figures 8d and 8e). Similarly, the Upper Midwest and south are among the regions with the highest projected changes in both cases. A predominant increase in the number of precipitation extremes across the U.S. is consistent with the projected changes in number of wet days that show a decline in almost all regions. The strongest median decline in wet days (−5 days/year, Figure 8f) occurs over the west and southwest, both of which show a median decrease in mean precipitation and a relatively smaller increase in number of precipitation extremes days (~1 every 2 years).

3.5. Changes in Snow Hydrology

We also examine the projected snow hydrology simulated by the land surface component of RegCM4. The magnitudes of cold season average snow depth, snow days, and their future changes, along with the changes in number of extreme snow events, and the timing of strongest warming are shown in Figure 9. Strongest warming is calculated as the maximum monthly departure from baseline temperatures across all the months. Historically, a substantial amount of cold season (October to March) precipitation falls in the form of snow across the U.S. (Figures 9a and 9b) with maxima over the Great Lakes region and the higher elevations in the western U.S. For the comparison of simulated snow with the station observation, we refer readers to *Naz et al*. [2016] that describes hydrologic model's results at 4 km over the conterminous U.S. when it is driven with the RCM-SUB data. In future projections, with a few exceptions over the north-central region, over 60% of the members of RCM-SUB simulate decreases in both the amount and number of snow days over the U.S. (represented by stippling). Decreases in snow days are strongest (>20%) over regions where major precipitation falls as rain, whereas decreases in snow amount are strongest (up to 15%) over higher elevations in the west where most of the precipitation falls as snow, particularly in the Sierra Nevada and Cascade Mountains (Figures 9c and 9d). Despite these projected changes in snow amount and days, many higher elevations in the west, northern Great Plains, Great Lakes, and Ohio Valley are expected to see an increase in snow extremes (up to 1 event per year) (Figure 9e). The possibility of an increase in total snow amount or snow extremes in future climates has also been reported in earlier studies [e.g., *Kapnick and Delworth*, 2013; *O'Gorman*, 2014], generally consistent with moister atmospheric conditions and relatively milder decreases in cold extremes in the future period (Figure 5c). Overall, these changes in snow hydrology have a profound impact on the timing of the strongest surface warming (Figure 9f) and perhaps on the magnitudes of projected surface warming. Higher elevations in the western U.S., where snow accumulates during the cold season (autumn/winter) and melts in the warm season (spring/summer), exhibit the strongest warming in the spring and summer months, consistent with the changes in snow amount over those regions (Figures 9c and 9d). A decrease in snow in the cold season reduces the amount of snow that is available for melt in the warm season, which advances the timing of a snow free land surface and therefore influences surface temperatures through changes in surface albedo. On the other hand, the Midwest, Ohio Valley, and northeast exhibit the strongest warming in the cold season where presently a major part of the cold season precipitation falls as snow but does not accumulate during the season and instead melts over several days after each snowfall episode. Therefore, any future warming that is related to changes in snow albedo occurs during the cold season as the overall amount of snow decreases (Figures 9c and 9d). These important relationships between changes in snow and surface warming projections in future climates across the U.S. should be noted while assessing the differences in magnitudes of warming between CMIP5 GCMs and a high-resolution RegCM4 ensemble.

3.6. Clausius-Clapeyron Scaling

We summarize the relationship between the increase in mean annual temperature and percent change in precipitation from wet extremes in Figure 10. The Clausius-Clapeyron relation suggests a 7% increase in the moisture holding capacity of the atmosphere per degree centigrade rise in temperature [*Trenberth et al*., 2003]. This

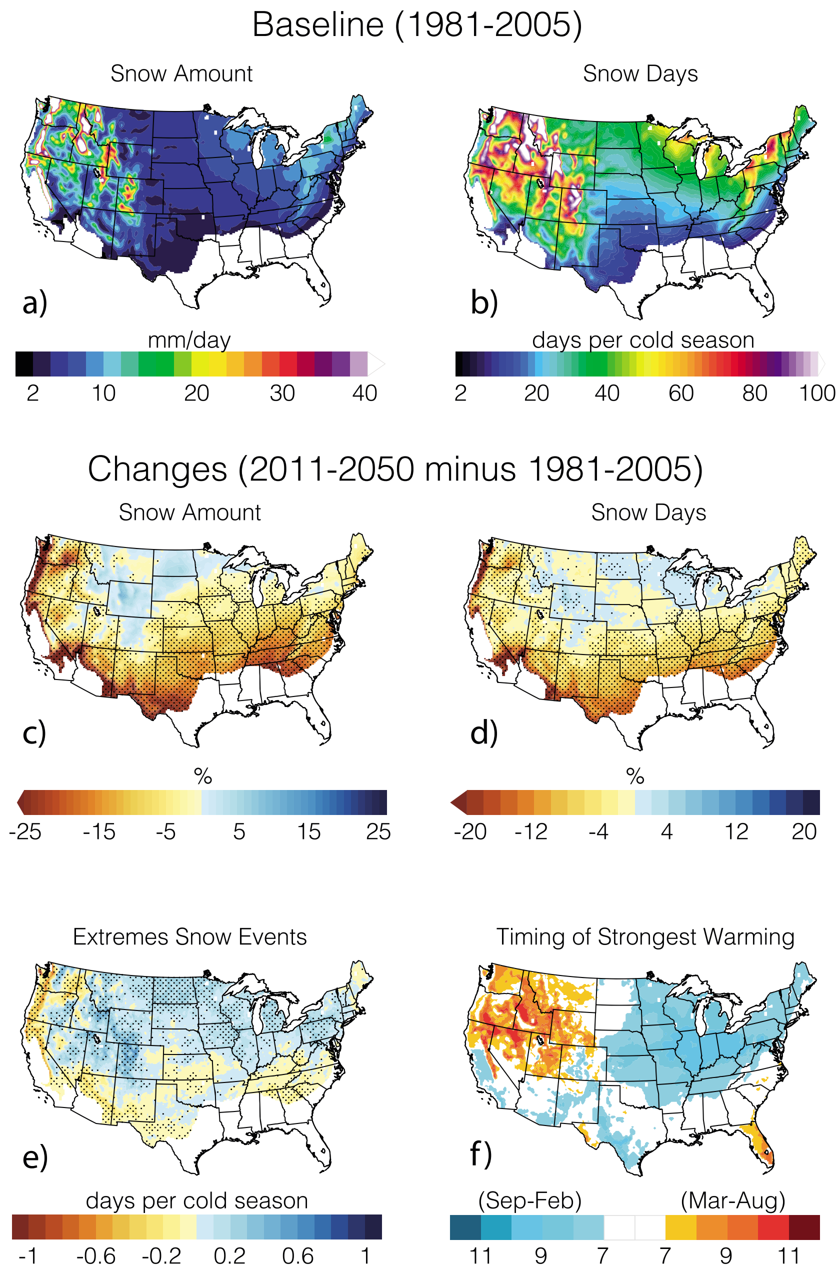

Figure 9. (a) Average snow amount (mm/day) and (b) number of snow days (days per cold season) in the cold season (October to March) of the baseline period (1981–2005). Projected changes in snow hydrology: (c) snow amount (%), (d) number of snow days (%), and (e) number of extreme snow events (days per cold season). (f) Number of models at each grid point that exhibit strongest future warming either in the months that experience snow (blue) or in the months that experience melting of accumulated snow (red). Strongest warming is calculated as maximum monthly departure from baseline temperatures across all the months.

means that in the absence of other dynamical forcing and given that almost all of the atmospheric moisture is expected to be converted to precipitation during an extreme event, extreme precipitation should increase at a comparable rate (7% per °C increase). Studies have shown that scaling of extreme precipitation magnitudes also depends on the time scale over which event is being measured (e.g., daily and hourly), storm type (e.g., large-scale versus convective), location (e.g., orographic effects on moisture transport), resulting in increases that vary from < 7% to 14% in the observations [e.g., *Berg et al.*, 2013; *Haerter and Berg*, 2009; *Lenderink and Van Meijgaard*, 2008; *Singleton and Toumi*, 2013]. In our analysis, both cold season precipitation extremes (snow) driven by large-scale weather systems and hot season precipitation extremes driven

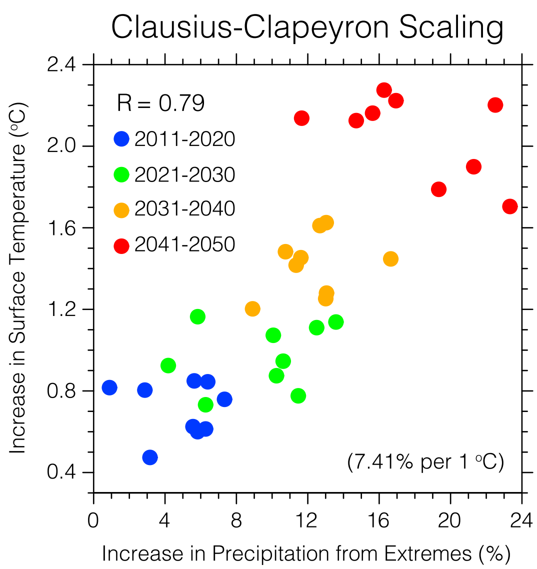

Figure 10. Relationship between the increase in the surface temperature and the increase in the percent of precipitation falling as extremes. Each dot represents 10 years spatially averaged over one of the nine NCEI climate regions. Colors represent one of the four decades in the future period.

by fine-scale convection are showing an increase across the U.S. along with a rise in temperature (Figures 5 and 9). At a regional scale, we find a strong relationship ($R = 0.79$) between the increase in temperature and percent increase in the amount of daily precipitation falling as extreme with a 7.4% increase in the percent of precipitation contributed by daily extremes per °C rise in temperature. While we expect this relationship to vary between 7 and 14% at subdaily and grid-scale levels, as evident in observations based studies, it nevertheless depicts a general consistency with previous findings and provides a first-order estimate of how changes in regional scale extremes may scale with increasing temperatures across the U.S. in the coming decades given that regional-scale warming remains below 2°C for most of the projection period.

3.7. Transient Climate Change

We present the time series of anomalies of temperature and precipitation characteristics with reference to the 1981–2005 for which gridded daily observations are available (Figures 11 and 12). Anomalies are calculated at each grid point in the individual baseline and future years by subtracting the 25 year average of the reference period and the results are presented as spatial averages of the projected anomalies using all the grid points within a NCEI region. The grey lines in Figures 11 and 12 represent individual ensemble members, the thick black and red lines represent the ensemble mean in the baseline and future periods, respectively, and the green and blue lines represent the PRISM and Daymet observations, respectively. We extend the observed anomalies to 2012 to provide a reference for the future trajectory of the projected trends.

All climate regions are projected to reach 2°C warming by mid-21st century with more accelerated pace of warming over the southwest, west, and northwest and a slower pace of warming over the south and southeast (Figure 11a). It is important to note that the historical trends in the baseline period and the projected pace of warming in RCM-SUB follows the observed warming trends with the exception of the northeast where observed warming trends are apparently stronger than the simulated trends, which could be in part due to relatively lower skill in RCM-SUB over that region (Figures 3 and 4). Progressive warming trends in the mean annual temperatures are associated with consistent decreasing trends in the number of cold extremes and increasing trends in the number of hot extremes (Figures 11b and 11c). Many of the regions, including the southwest, west, and southeast are already showing an increase in the occurrence of hot extremes in the observations. Similarly, observations exhibit strong decreasing trends in the number of cold extremes over the northwest and northeast. Our simulations suggest an intensification of such trends in the coming decades. It should be noted that both in the observations and simulations, year-to-year variations in the number of hot extremes is much stronger than those in the number of cold extremes, which is also consistent with the relatively stronger interensemble spread in the number of hot extremes compared to that in the change of cold extreme days (Figure 8). However, it appears that RCM-SUB tends to overestimate hot extremes in the first few years (more visible in the western half of the U.S.) of the future period before equilibrating toward a trajectory of lower magnitude. Similar but less pronounced behavior also exists in the baseline period (Figure 11c). This can either be due to an undocumented fact that RCMs tend to take much longer than expected to equilibrate when simulating hot extremes or due to a bias internal to RegCM4.

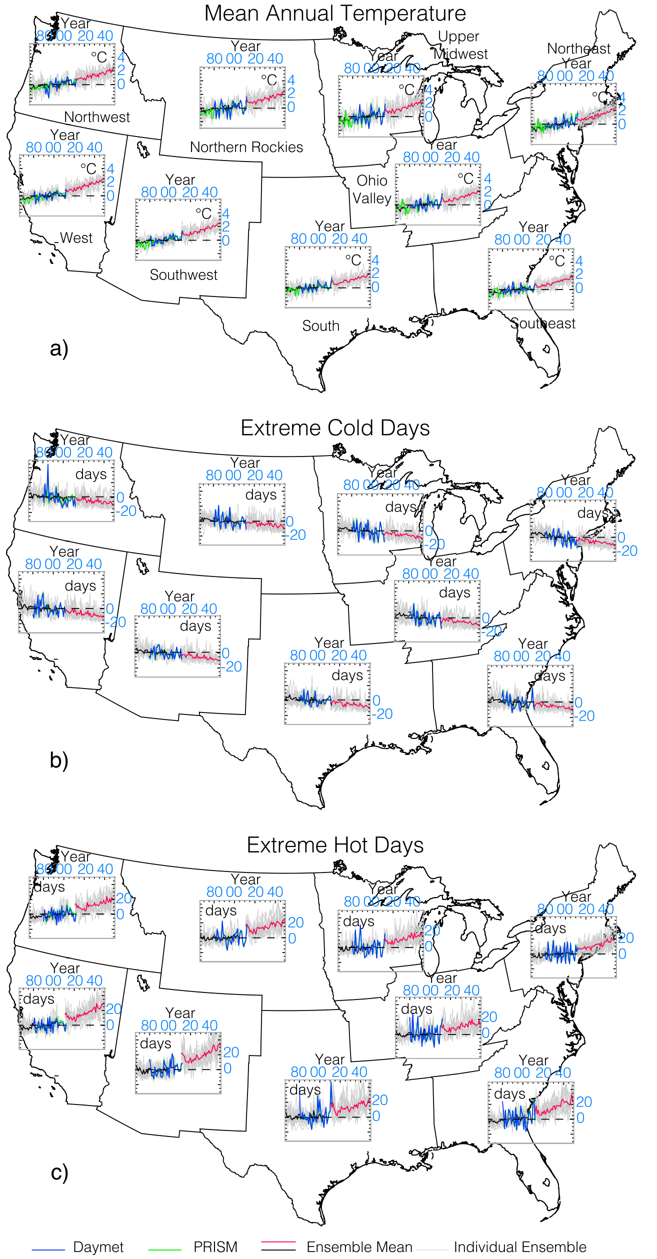

Figure 11. Annual anomalies with respect to 1981–2005 reference period in (a) annual surface temperatures (°C), (b) number of extreme cold days, and (c) number of extreme hot days. Anomalies are calculated at each grid point in the individual baseline and the future years by subtracting the 25 year average of the reference period and the results are presented as spatial averages of the projected anomalies using all the grid points within a NCEI region. The grey lines represent individual members in RCM-SUB, the black and red lines represent the ensemble mean in the baseline and future periods, respectively, and the green and blue lines represent anomalies in the PRISM and the Daymet observations, respectively. We extend the observed anomalies to 2012 to provide a reference for the future trajectory of the projected trends.

As suggested by the long-term mean changes in the annual mean precipitation in Figure 5d, three northern climate regions (northwest, Upper Midwest, and northern Rockies) show progressive positive precipitation trends in the future period and one climate region (southwest) shows a progressive negative trend (Figure 12a). The interannual variability in the observed anomalies in the baseline period generally remains within the RCM-SUB spread with the west exhibiting the largest variability in both the observations and the simulations (Figure 12a). Observations also show a prevailing negative trend over the southwest region; however, the magnitude of the trend is much stronger in the observations than that in the simulations. Regardless of the trends in the mean annual precipitation, the number of daily precipitation extremes shows a positive trend over all regions in the projections (Figure 12b). Many regions show an increase of up to 20% in the number of daily precipitation extremes by the mid-21st century, with the southeast and northwest exhibiting some of the strongest trends. It is important to note that over many regions, including the northeast, southwest, southeast, and northern Rockies, PRISM observations show a strong increasing trend in the occurrence of daily precipitation extremes during the first decade of the 21st century, but with the exception of the northeast, no such trends are observed in the Daymet observations. We can attribute this difference in trends to the fact that PRISM precipitation observations have made use of radar data in the recent years, while Daymet solely relies on ground observations. Similar increasing trends to PRISM were also reported in the third National Climate Assessment Report [*Melillo et al.*, 2014]. In light of the apparent discrepancy between the two observational data sets, the projected trajectory of the simulated trends in the number of daily precipitation extremes are either consistent or milder than the current observed trends over most of the regions (Figure 12b). Some of the differences in the trajectories of changes in daily precipitation extremes in the

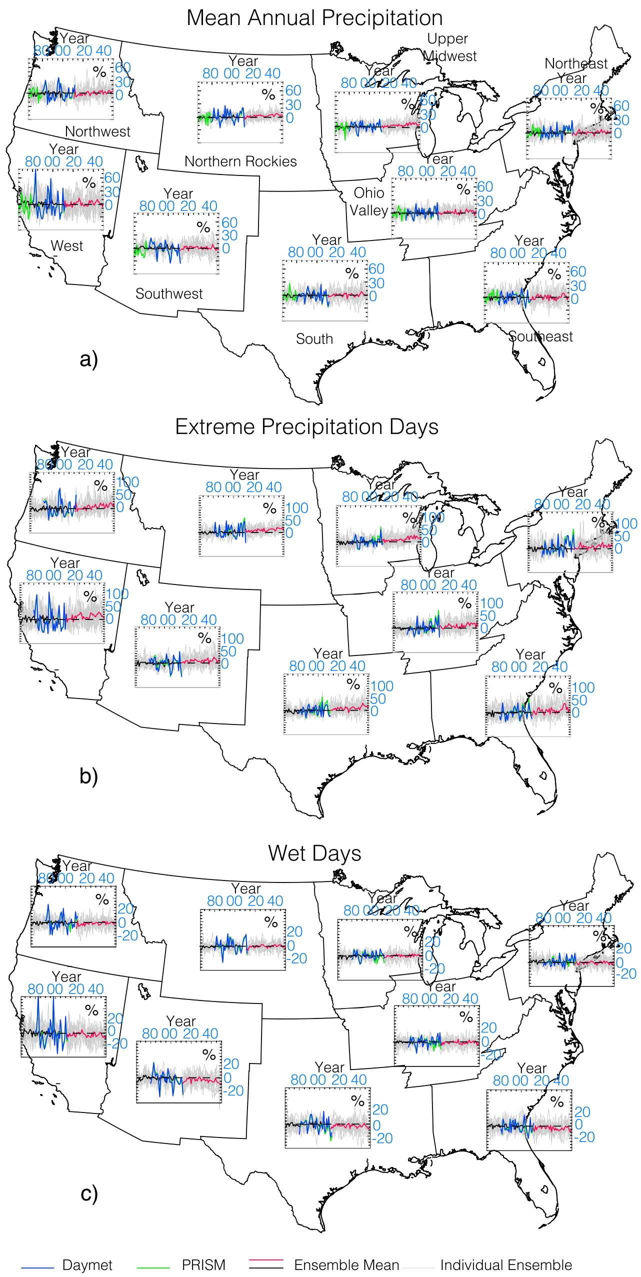

Figure 12. Same as in Figure 11 but for annual precipitation, extreme precipitation days and wet days.

Daymet and PRISM observations during the first decade of the 21st century can be attributed to their differences in the trajectory of changes in the number of wet days, e.g., over Ohio Valley and Upper Midwest (Figures 12b and 12c). In RCM-SUB, the projected changes in the mean annual precipitation and the increasing trends in the number of daily precipitation extremes across all regions are consistent with the trajectory of changes in the number of wet days (Figure 12c). Many regions, including the southwest, south, southeast, and west that exhibit strong increasing trends in the number of precipitation extremes also show a decreasing trend in the number of wet days in the coming decades. On the other hand, regions (northwest, northern Rockies, and Upper Midwest) that exhibit an increasing trend in mean annual precipitation are projected to have little to no change in the number of wet days in a given year.

4. Summary and Conclusions

Using a dynamical downscaling framework, we provide high-resolution ensemble climate projections over the continental U.S. Most of our analyses are summarized in Figure 13. Observations provide discernable evidence that the hydrological cycle is changing over the U.S. Statistically significant warming trends—a key driver of the water cycle intensification—are visible over many regions across the U.S., including the northeast, west, southwest, and northwest (Figure 13). Associated with this warming, the northeast and northwest also exhibit significant decreasing trends in the cold extremes. Similarly, hot extremes have significantly increased over the southwest at the cost of a significant decrease in the number of precipitation days and the magnitudes of annual precipitation.

All the significant trends in mean annual and extreme cold daily temperatures are also simulated by the RCM-SUB, shown as arrows with the dotted lines in Figure 13. Without any intervention in the present trajectory of the greenhouse gas emissions, average warming trends over the four decades (2011–2050) are expected to be between 1–2°C across the U.S. (Figure 13). However, every region in the continental U.S. will start experiencing a frequent occurrence of years with magnitudes of warming 2°C or greater before the mid-21st century (Figure 11a). With the exception of regions that represent the present-day warming hole in the parts of the midwest, Ohio Valley, and south, all regions are expected to experience statistically significant increase in

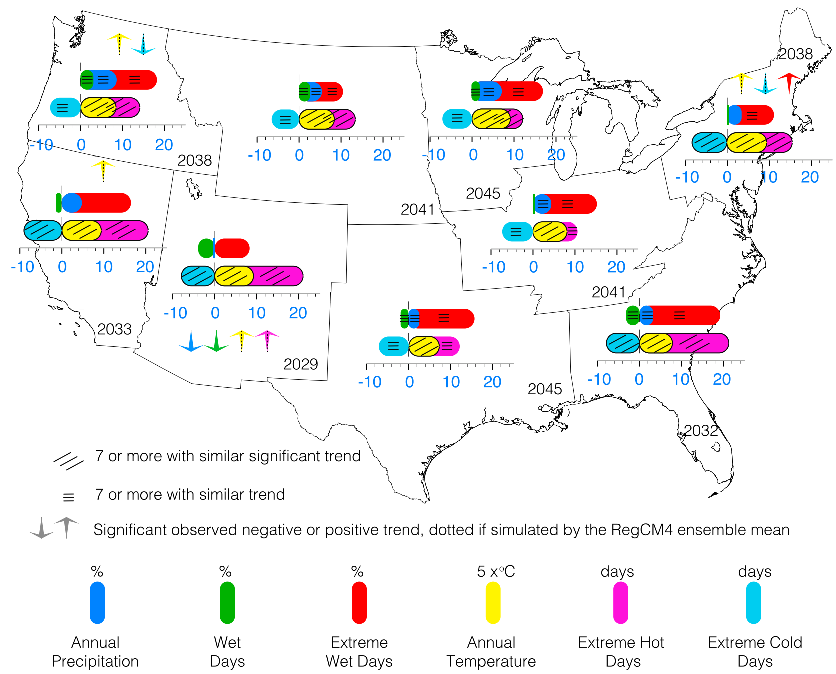

Figure 13. Summary of the results over each of the nine NCEI regions. Each color represents a unique variable. Arrows represent the regions where both PRISM and Daymet exhibit statistically significant trend in the baseline period. Arrows are dotted if similar and statistically significant trends are exhibited in the corresponding baseline period of RCM-SUB. Horizontal color bars with diagonal lines represent the regions where seven or more members of RCM-SUB exhibit similar and statistically significant trends in the future period. Horizontal color bars with horizontal lines represent the regions where seven or more members of RCM-SUB exhibit similar but statistically insignificant trend in the future period. Horizontal color bars without any lines represent the regions where less than seven ensemble members exhibit similar or significant trends in the future period. Numbers in each region represent the year when projected surface warming is above the baseline variability (> baseline standard deviation of annual mean temperature).

days when maximum daily temperatures exceed the 95th percentile of their historical daily threshold (at least >12 days per year, Figure 13). In the south and Ohio Valley, most of the precipitation increase occurs later during the hydrological year in the form of excess warm season rainfall, which is reflected in the delay in the timing of 50% of the annual precipitation during a hydrological year (Figure 6d). This excessive warm season rainfall should partly help limit the increase in the frequency of daily hot extremes, which explains the lack of significant trends in hot extremes in these regions. A decrease in cold temperature extremes is also expected across the U.S.; however, these trends are only significant over the southeast, northeast, west, and southwest. It is important to note that regions with significant trends in both hot and cold extremes are also the ones that are expected to reach a warming level beyond the baseline variability before 2040, shown as the numbers in each region in Figure 13, meaning that both milder winters and hotter summers are needed for accelerated warming.

Theoretically, a 1–2°C average warming should expect to produce mean annual and extreme daily precipitation changes up to 5–10% and 10–20%, respectively [e.g., *Berg et al.*, 2013; *Haerter and Berg*, 2009; *Held and Soden*, 2006; *Lenderink and Van Meijgaard*, 2008; *Muller et al.*, 2011; *Singleton and Toumi*, 2013; *Stephens and Hu*, 2010], meaning that a significant trend in mean and extreme precipitation changes is highly unlikely in the next few decades. Our projections are consistent with the theoretical understandings both in magnitude and the statistical insignificance of precipitation trends. However, with the exception of the west and southwest, the future trajectory of trends is consistent across the members of RCM-SUB (Figures 12 and 13), meaning that the emergence of significant precipitation trends beyond the mid-21st century is quite a possibility. Moreover, it is important to note that observed hydrometrological anomalies (prevailing drought) over the southwest and California are predominantly driven by the observed significant warming trends [*Diffenbaugh et al.*, 2015; *Swain et al.*, 2014]. Since RCM-SUB exhibits significant future trends in both mean and extreme temperatures over these regions, inconsistencies in precipitation projections do not necessarily reduce the likelihood of the inherent climate risk associated with warmer temperature.

Snow hydrology apparently plays a critical role in regulating the temperature response over the regions that receive a significant portion of cold season precipitation in the form of snow, consistent with the observations [e.g., *Groisman et al*., 1994]. Decreases in snow-covered area expose more land surface with much lower albedo, accelerating the rate of surface warming. On the other hand, a reduction in snow days reduces the number of days with fresh snow on the ground, which has a higher albedo than old snow. Alternatively, warmer temperatures accelerate the rate of snowmelt, which further decreases surface albedo, as melting snow albedo is less than frozen or dry snow albedo. Overall, our results indicate that such changes in snow hydrology can determine the magnitudes and timing of surface warming by altering the surface energy budget through the snow albedo feedback (Figure 9). Nonetheless, projected changes in hydroclimate across the U.S. can have profound impacts on natural and human systems, including snow dominated water resources, hydropower generation, tree mortality, and forest fires [e.g., *Ashfaq et al*., 2013; *Barnett et al*., 2005; *Diffenbaugh et al*., 2015; *Kao et al*., 2015; *Williams et al*., 2013].

Overall, the RCM-SUB simulations provide a comprehensive and detailed understanding of the potential changes in the regional climate over the U.S. However, we acknowledge the fact that dynamically downscaled climate projections are sensitive to the choice of the regional climate model [e.g., *Ayar et al*., 2016] particularly in the simulation of warm season precipitation and convectively driven regional-scale circulations. Therefore, despite the use of a large number of driving GCMs, the use of a single RCM in our modeling setup limits its ability to capture the model based uncertainties associated with RCM internal biases and convective parameterizations [e.g., *Alexandru et al*., 2007; *Giorgi and Gutowski*, 2015]. Nonetheless, we expect these simulations to be useful for comparison with other approaches involving statistical downscaling, dynamical downscaling using different RCMs, high-resolution GCMs, and high-resolution variable resolution GCMs and should help toward the development of robust climate modeling approaches for understanding climate change and its impacts at regional and local scales. Efforts are in progress to make parts of this data available for the scientific community through Oak Ridge National Laboratory (ORNL)'s National Extreme Events Data and Research Center (NEED).

Acknowledgments
We thank three anonymous reviewers for their constructive and insightful comments. This study was funded by the Regional and Global Climate Modeling Program within the Office of Science and the Wind and Water Power Technologies Office within Office of Energy Efficiency and Renewable Energy of the U.S. Department of Energy (DOE), and also the Oak Ridge National Laboratory (ORNL) Laboratory Directed Research and Development Program. This paper was authored by employees of the ORNL, managed by UT Battelle, LLC, under contract DE-AC05-00OR22725 with the U.S. DOE. Accordingly, the publisher, by accepting the article for publication, acknowledges that the United States government retains a nonexclusive, paid-up, irrevocable, worldwide license to publish or reproduce the published form of this manuscript, or allow others to do so, for United States government purposes. Support for RegCM4 simulations, data storage, and analysis is provided by the Oak Ridge Leadership Computing Facility, and this data can be obtained by contacting M. Ashfaq (mashfaq@ornl.gov) at ORNL Climate Change Science Institute. We also thank U.S. DOE's Program for Climate Model Diagnosis and Intercomparison for providing coordinating support and leading development of software infrastructure in partnership with the Global Organization for Earth System Science Portals for CMIP.

References

Alexandru, A., R. de Elia, and R. Laprise (2007), Internal variability in regional climate downscaling at the seasonal scale, *Moon Weather Rev.*, *135*(9), 3221–3238, doi:10.1175/Mwr3456.1.

Ashfaq, M., Y. Shi, W. W. Tung, R. J. Trapp, X. J. Gao, J. S. Pal, and N. S. Diffenbaugh (2009), Suppression of south Asian summer monsoon precipitation in the 21st century, *Geophys. Res. Lett.*, *36*, L01704, doi:10.1029/2008GL036500.

Ashfaq, M., L. C. Bowling, K. Cherkauer, J. S. Pal, and N. S. Diffenbaugh (2010), Influence of climate model biases and daily-scale temperature and precipitation events on hydrological impacts assessment: A case study of the United States, *J. Geophys. Res.*, *115*, D14116, doi:10.1029/2009JD012965.

Ashfaq, M., S. Ghosh, S. C. Kao, L. C. Bowling, P. Mote, D. Touma, S. A. Rauscher, and N. S. Diffenbaugh (2013), Near-term acceleration of hydroclimatic change in the western US, *J. Geophys. Res. Atmos.*, *118*, 10,676–10,693, doi:10.1002/jgrd.50816.

Ayar, P. V., M. Vrac, S. Bastin, J. Carreau, M. Deque, and C. Gallardo (2016), Intercomparison of statistical and dynamical downscaling models under the EURO- and MED-CORDEX initiative framework: Present climate evaluations, *Clim. Dyn.*, *46*(3-4), 1301–1329, doi:10.1007/s00382-015-2647-5.

Barnett, T. P., J. C. Adam, and D. P. Lettenmaier (2005), Potential impacts of a warming climate on water availability in snow-dominated regions, *Nature*, *438*(7066), 303–309, doi:10.1038/nature04141.

Berg, P., C. Moseley, and J. O. Haerter (2013), Strong increase in convective precipitation in response to higher temperatures, *Nat. Geosci.*, *6*(3), 181–185, doi:10.1038/ngeo1731.

Daly, C., M. Halbleib, J. I. Smith, W. P. Gibson, M. K. Doggett, G. H. Taylor, J. Curtis, and P. P. Pasteris (2008), Physiographically sensitive mapping of climatological temperature and precipitation across the conterminous United States, *Int. J. Climatol.*, *28*(15), 2031–2064, doi:10.1002/joc.1688.

Diffenbaugh, N. S., and M. Ashfaq (2010), Intensification of hot extremes in the United States, *Geophys. Res. Lett.*, *37*, L15701, doi:10.1029/2010GL043888.

Diffenbaugh, N. S., J. S. Pal, R. J. Trapp, and F. Giorgi (2005), Fine-scale processes regulate the response of extreme events to global climate change, *Proc. Natl. Acad. Sci. U.S.A.*, *102*(44), 15,774–15,778, doi:10.1073/pnas.0506042102.

Diffenbaugh, N. S., M. Ashfaq, and M. Scherer (2011), Transient regional climate change: Analysis of the summer climate response in a high-resolution, century-scale ensemble experiment over the continental United States, *J. Geophys. Res.*, *116*, D24111, doi:10.1029/2011JD016458.

Diffenbaugh, N. S., D. L. Swain, and D. Touma (2015), Anthropogenic warming has increased drought risk in California, *Proc. Natl. Acad. Sci. U.S.A.*, *112*(13), 3931–3936, doi:10.1073/pnas.1422385112.

Duffy, P. B., R. W. Arritt, J. Coquard, W. Gutowski, J. Han, J. Iorio, J. Kim, L. R. Leung, J. Roads, and E. Zeledon (2006), Simulations of present and future climates in the western United States with four nested regional climate models, *J. Clim.*, *19*(6), 873–895, doi:10.1175/Jcli3669.1.

Fan, F. X., R. S. Bradley, and M. A. Rawlins (2014), Climate change in the northeastern US: Regional climate model validation and climate change projections, *Clim. Dyn.*, *43*(1-2), 145–161, doi:10.1007/s00382-014-2198-1.

Feng, X., A. Porporato, and I. Rodriguez-Iturbe (2013), Changes in rainfall seasonality in the tropics, *Nat. Clim. Change*, *3*(9), 811–815, doi:10.1038/Nclimate1907.

Fritsch, J. M., and C. F. Chappell (1980), Numerical prediction of convectively driven mesoscale pressure systems 1. Convective parameterization, *J. Atmos. Sci.*, *37*(8), 1722–1733, doi:10.1175/1520-0469(1980)037<1722:Npocdm>2.0.Co;2.

Giorgi, F., and W. J. Gutowski (2015), Regional Dynamical Downscaling and the CORDEX Initiative, *Annu. Rev. Environ. Resour.*, *40*, 467–490, doi:10.1146/annurev-environ-102014-021217.

Giorgi, F., and L. O. Mearns (1999), Introduction to special section: Regional climate modeling revisited, *J. Geophys. Res.*, *104*, 6335–6352, doi:10.1029/98JD02072.

Giorgi, F., et al. (2012), RegCM4: Model description and preliminary tests over multiple CORDEX domains, *Clim. Res.*, *52*(1), 7–29, doi:10.3354/cr01018.

Grell, G. A. (1993), Prognostic evaluation of assumptions used by cumulus parameterizations, *Mon. Weather Rev.*, *121*(3), 764–787, doi:10.1175/1520-0493(1993)121<0764:Peoaub>2.0.Co;2.

Grell, G. A., A. J. Dudhia, and D. R. Stauffer (1994), A description of the fifth-generation Penn State/NCAR mesoscale model (MM5), *NCAR Tech. Note NCAR/TN-398+STR*, Natl. Cent. for Atmos. Res., Boulder, Colo.

Groisman, P. Y., T. R. Karl, R. W. Knight, and G. L. Stenchikov (1994), Changes of snow cover, temperature, and radiative heat-balance over the Northern-Hemisphere, *J. Clim.*, *7*(11), 1633–1656, doi:10.1175/1520-0442(1994)007<1633:Coscta>2.0.Co;2.

Gula, J., and W. R. Peltier (2012), Dynamical Downscaling over the Great Lakes Basin of North America using the WRF Regional Climate Model: The impact of the Great Lakes System on regional greenhouse warming, *J. Clim.*, *25*(21), 7723–7742, doi:10.1175/Jcli-D-11-00388.1.

Haerter, J. O., and P. Berg (2009), Unexpected rise in extreme precipitation caused by a shift in rain type?, *Nat. Geosci.*, *2*(6), 372–373, doi:10.1038/ngeo523.

Hagos, S., L. R. Leung, Q. Yang, C. Zhao, and J. Lu (2015), Resolution and Dynamical Core Dependence of Atmospheric River Frequency in Global Model Simulations, *J. Clim.*, *28*(7), 2764–2776, doi:10.1175/Jcli-D-14-00567.1.

Held, I. M., and B. J. Soden (2006), Robust responses of the hydrological cycle to global warming, *J. Clim.*, *19*(21), 5686–5699, doi:10.1175/Jcli3990.1.

Holtslag, A. A. M., E. I. F. Debruijn, and H. L. Pan (1990), A High-Resolution Air-Mass Transformation Model for Short-Range Weather Forecasting, *Moon Weather Rev.*, *118*(8), 1561–1575, doi:10.1175/1520-0493(1990)118<1561:Ahramt>2.0.Co;2.

Houghton, J. T., G. J. Jenkins, and J. J. Ephraums (Eds.) (1990), *Climate Change: The IPCC Scientific Assessment*, 410 pp., Cambridge Univ. Press, Cambridge, New York.

Intergovernmental Panel on Climate Change (2013), *Climate Change 2013: The Physical Science Basis. Contribution of Working Group I to the Fifth Assessment Report of the Intergovernmental Panel on Climate Change*, edited by T. F. Stocker et al., 1535 pp., Cambridge Univ. Press, Cambridge, U. K., and New York, doi:10.1017/CBO9781107415324.

Kao, S. C., M. J. Sale, M. Ashfaq, R. U. Martinez, D. P. Kaiser, Y. X. Wei, and N. S. Diffenbaugh (2015), Projecting changes in annual hydropower generation using regional runoff data: An assessment of the United States federal hydropower plants, *Energy*, *80*, 239–250, doi:10.1016/j.energy.2014.11.066.

Kapnick, S. B., and T. L. Delworth (2013), Controls of Global Snow under a Changed Climate, *J. Clim.*, *26*(15), 5537–5562, doi:10.1175/Jcli-D-12-00528.1.

Karl, T. R., and W. J. Koss (1984), *Regional and National Monthly, Seasonal, and Annual Temperature Weighted by Area, 1895–1983*, *Historical Climatology Series 4-3*, Natl. Clim. Data Center, Asheville, N. C.

Kendall, M. G. (1975), *Rank Correlation Methods*, 4th ed., Charles Griffin, London.

Kiehl, J. T., J. J. Hack, G. B. Bonan, B. A. Boville, D. L. Williamson, and P. J. Rasch (1998), The National Center for Atmospheric Research Community Climate Model: CCM3, *J. Clim.*, *11*(6), 1131–1149, doi:10.1175/1520-0442(1998)011<1131:Tncfar>2.0.Co;2.

Lenderink, G., and E. Van Meijgaard (2008), Increase in hourly precipitation extremes beyond expectations from temperature changes, *Nat. Geosci.*, *1*(8), 511–514, doi:10.1038/ngeo262.

Leung, L. R., and Y. Qian (2003), The sensitivity of precipitation and snowpack simulations to model resolution via nesting in regions of complex terrain, *J. Hydrometeorol.*, *4*(6), 1025–1043, doi:10.1175/1525-7541(2003)004<1025:Tsopas>2.0.Co;2.

Liang, X. Z., K. E. Kunkel, G. A. Meehl, R. G. Jones, and J. X. L. Wang (2008), Regional climate models downscaling analysis of general circulation models present climate biases propagation into future change projections, *Geophys. Res. Lett.*, *35*, L08709, doi:10.1029/2007GL032849.

Lu, J., L. Leung, Q. Yang, G. Chen, W. D. Collins, F. Y. Li, Z. J. Hou, and X. L. Feng (2014), The robust dynamical contribution to precipitation extremes in idealized warming simulations across model resolutions, *Geophys. Res. Lett.*, *41*, 2971–2978, doi:10.1002/2014GL059532.

Mann, H. B. (1945), Nonparametric Tests against Trend, *Econometrica*, *13*(3), 245–259, doi:10.2307/1907187.

Mearns, L. O., W. J. Gutowski, R. Jones, L.-Y. Leung, S. McGinnis, A. M. B. Nunes, and Y. Qian (2009), A regional climate change assessment program for North America, *Eos Trans. AGU*, *90*(36), 2, doi:10.1029/2009EO360002.

Mearns, L. O., et al. (2012), The North American Regional Climate Change Assessment Program Overview of Phase I Results, *Bull. Am. Meteorol. Soc.*, *93*(9), 1337–1362.

Meehl, G. A., C. Tebaldi, G. Walton, D. Easterling, and L. McDaniel (2009), Relative increase of record high maximum temperatures compared to record low minimum temperatures in the U. S, *Geophys. Res. Lett.*, *36*, L23701, doi:10.1029/2009GL040736.

Meir, P., P. Cox, and J. Grace (2006), The influence of terrestrial ecosystems on climate, *Trends Ecol. Evol.*, *21*(5), 254–260, doi:10.1016/j.tree.2006.03.005.

Melillo, J. M., T. C. Richmond, and G. W. Yohe (Eds.) (2014), *Climate Change Impacts in the United States: The Third National Climate Assessment*, U.S. Global Change Research Program, 841 pp., U.S. Gov. Print. Off., Washington, D. C., doi:10.7930/J0Z31WJ2.

Moss, R. H., et al. (2010), The next generation of scenarios for climate change research and assessment, *Nature*, *463*(7282), 747–756, doi:10.1038/nature08823.

Muller, C. J., P. A. O'Gorman, and L. E. Back (2011), Intensification of Precipitation Extremes with Warming in a Cloud-Resolving Model, *J. Clim.*, *24*(11), 2784–2800, doi:10.1175/2011jcli3876.1.

Naz, B. S., S.-C. Kao, M. Ashfaq, D. Rastogi, R. Mei, and L. C. Bowling (2016), Regional hydrologic response to climate change in the conterminous United States using high-resolution hydroclimate simulations, *Global Planet. Change*, *143*, 100–117, doi:10.1016/j.gloplacha.2016.06.003.

O'Gorman, P. A. (2014), Contrasting responses of mean and extreme snowfall to climate change, *Nature*, *512*(7515), 416–418, doi:10.1038/nature13625.

Pal, J. S., E. E. Small, and E. A. B. Eltahir (2000), Simulation of regional-scale water and energy budgets: Representation of subgrid cloud and precipitation processes within RegCM, *J. Geophys. Res.*, *105*, 29,579–29,594, doi:10.1029/2000JD900415.

Pal, J. S., et al. (2007), Regional climate modeling for the developing world - The ICTP RegCM3 and RegCNET, *Bull. Am. Meteorol. Soc.*, *88*(9), 1395–1409, doi:10.1175/Bams-88-9-1395.

Peters, G. P., R. M. Andrew, T. Boden, J. G. Canadell, P. Ciais, C. Le Quere, G. Marland, M. R. Raupach, and C. Wilson (2013), COMMENTARY: The challenge to keep global warming below 2 degrees C, *Nat. Clim. Change*, *3*(1), 4–6.

Plummer, D. A., D. Caya, A. Frigon, H. Cote, M. Giguere, D. Paquin, S. Biner, R. Harvey, and R. De Elia (2006), Climate and climate change over North America as simulated by the Canadian RCM, *J. Clim.*, *19*(13), 3112–3132, doi:10.1175/Jcli3769.1.

Portmann, R. W., S. Solomon, and G. C. Hegerl (2009), Spatial and seasonal patterns in climate change, temperatures, and precipitation across the United States, *Proc. Natl. Acad. Sci. U.S.A.*, *106*(18), 7324–7329, doi:10.1073/pnas.0808533106.

Salathe, E. P., L. R. Leung, Y. Qian, and Y. X. Zhang (2010), Regional climate model projections for the State of Washington, *Clim. Change*, *102*(1-2), 51–75, doi:10.1007/s10584-010-9849-y.

Singleton, A., and R. Toumi (2013), Super-Clausius-Clapeyron scaling of rainfall in a model squall line, *Q. J. R. Meteorol. Soc.*, *139*(671), 334–339, doi:10.1002/qj.1919.

Stephens, G. L., and Y. X. Hu (2010), Are climate-related changes to the character of global-mean precipitation predictable?, *Environ. Res. Lett.*, *5*(2), doi:10.1088/1748-9326/5/2/025209.

Suggitt, A. J., P. K. Gillingham, J. K. Hill, B. Huntley, W. E. Kunin, D. B. Roy, and C. D. Thomas (2011), Habitat microclimates drive fine-scale variation in extreme temperatures, *Oikos*, *120*(1), 1–8, doi:10.1111/j.1600-0706.2010.18270.x.

Swain, D. L., M. Tsiang, M. Haugen, D. Singh, A. Charland, B. Rajaratnam, and N. S. Diffenbaugh (2014), The Extraordinary California Drought of 2013/2014: Character, Context, and the Role of Climate Change, *Bull. Am. Meteorol. Soc.*, *95*(9), S3–S7.

Tawfik, A. B., and A. L. Steiner (2011), The role of soil ice in land-atmosphere coupling over the United States: A soil moisture-precipitation winter feedback mechanism, *J. Geophys. Res.*, *116*, D02113, doi:10.1029/2010JD014333.

Taylor, K. E. (2001), Summarizing multiple aspects of model performance in single diagram, *J. Geophys. Res.*, *106*, 7183–7192, doi:10.1029/2000JD900719.

Thornton, P. E., M. M. Thornton, B. W. Mayer, N. Wilhelmi, Y. Wei, A. R. Devarakonda, and R. B. Cook (2014), *Daymet: Daily Surface Weather Data on a 1-km Grid for North America*, *Version 2*, ORNL DAAC, Tennessee.

Trenberth, K. E., A. Dai, R. M. Rasmussen, and D. B. Parsons (2003), The changing character of precipitation, *Bull. Am. Meteorol. Soc.*, *84*(9), 1205–1217, doi:10.1175/Bams-84-9-1205.

Walker, M. D., and N. S. Diffenbaugh (2009), Evaluation of high-resolution simulations of daily-scale temperature and precipitation over the United States, *Clim. Dyn.*, *33*(7-8), 1131–1147, doi:10.1007/s00382-009-0603-y.

Wehner, M. F., R. L. Smith, G. Bala, and P. Duffy (2010), The effect of horizontal resolution on simulation of very extreme US precipitation events in a global atmosphere model, *Clim. Dyn.*, *34*(2-3), 241–247, doi:10.1007/s00382-009-0656-y.

Williams, A. P., et al. (2013), Temperature as a potent driver of regional forest drought stress and tree mortality, *Nat. Clim. Change*, *3*(3), 292–297, doi:10.1038/Nclimate1693.